

High-order velocity structure functions in turbulent shear flows

By F. ANSELMET, Y. GAGNE, E. J. HOPFINGER

Laboratoire Associé au CNRS, Institut de Mécanique,
Université Scientifique et Médicale de Grenoble,
38402 Saint Martin d'Hères, France

AND R. A. ANTONIA

Department of Mechanical Engineering, University of Newcastle, N.S.W., 2308, Australia

(Received 16 April 1983)

Measurements are presented of the velocity structure function on the axis of a turbulent jet at Reynolds numbers $R_\lambda \leq 852$ and in a turbulent duct flow at $R_\lambda = 515$. Moments of the structure function up to the eighteenth order were calculated, primarily with a view to establish accurately the dependence on the order of the inertial range power-law exponent and to draw conclusions about the distribution of energy transfer in the inertial range. Adequate definition of the probability density of the structure function was achieved only for moments of order $n \leq 10$. It is shown, however, that, although the values of moments of $n > 10$ diverges from their true values, the dependence of the moment of the structure function on the separation r is still given to a fair accuracy for moments up to $n \approx 18$. The results demonstrate that the inertial-range power-law exponent is closely approximated by a quadratic dependence on the power which for lower-order moments ($n \lesssim 12$) would be consistent with a lognormal distribution. Higher-order moments diverge, however, from a lognormal distribution, which gives weight to Mandelbrot's (1971) conjecture that 'Kolmogorov's third hypothesis' is untenable in the strict sense. The intermittency parameter μ , appearing in the power-law exponent, has been determined from sixth-order moments $\langle (\Delta u)^6 \rangle \sim r^{2-\mu}$ to be $\mu = 0.2 \pm 0.05$. This value coincides with that determined from non-centred dissipation correlations measured in identical conditions.

1. Introduction

Important modifications to Kolmogorov's (1941) local similarity theory were introduced in 1962 by Kolmogorov and Obukhov, who took into account spatial fluctuations in the turbulent energy dissipation ϵ . A specific form (lognormal) for the probability density of ϵ_r , the dissipation averaged over a volume of linear dimension r , was chosen. This choice, together with an assumed variation of the variance of $\ln \epsilon_r$, justified by Yaglom (1966), was described by Kolmogorov (1962) as a third hypothesis. The assumptions embodied in this hypothesis have often been referred to as the lognormal model (hereafter LN). Mandelbrot (1976) has pointed out that the lognormal assumption is only a special, probably physically unrealistic, case of weighted curdling. Physical models (e.g. Corrsin 1962; Tennekes 1968; Saffman 1968) based on particular geometries for the active regions, have also been proposed. Other models, such as the Novikov–Stewart (1964) model and the β -model of Frisch, Sulem

& Nelkin (1978) have been developed which differ from LN in that the approach taken is not based on a probabilistic model of the dissipation. Frisch *et al.* (1978) emphasised the fact that the β -model focuses on quantities, such as velocity amplitudes and the nonlinear energy transfer, in the inertial range. It has been pointed out (e.g. by Kraichnan 1974) that the dynamically relevant quantity is the nonlinear energy transfer and not the linear viscous dissipation.

Most of the previous models have led to predictions for the variation of statistical properties of turbulence with Reynolds number. The two most commonly reported properties are the structure functions, in particular the behaviour of their moments in the inertial range, and moments of the velocity derivative. We consider in this paper primarily the velocity structure function and restrict our attention to a comparison between LN and the β -model. The n th-order longitudinal velocity structure function may be written as

$$\langle (\Delta u)^n \rangle = \langle [u(x+r) - u(x)]^n \rangle.$$

When the separation lies in the inertial subrange

$$\langle \Delta u^n \rangle \sim r^{\frac{1}{3}n} \langle \epsilon^{\frac{1}{3}n} \rangle. \quad (1)$$

This can be obtained from energy-transfer considerations. Both LN and the β -model lead to

$$\langle \Delta u^n \rangle \sim \langle \epsilon \rangle^{\frac{1}{3}n} r^{\zeta_n}, \quad (2)$$

where

$$\zeta_n = \frac{1}{3}n - \mu_{\frac{1}{3}n},$$

but the departure $\mu_{\frac{1}{3}n}$ from the original similarity result is different for LN and the β -model. For LN, the dependence on n of $\mu_{\frac{1}{3}n}$ is quadratic,

$$\mu_{\frac{1}{3}n} = \frac{1}{15}\mu n(n-3), \quad (3)$$

whereas a linear dependence on n is obtained for the β -model, viz

$$\mu_{\frac{1}{3}n} = \frac{1}{3}\mu(n-3). \quad (4)$$

In (3) and (4), μ is the exponent in the inertial-range power-law behaviour of the autocorrelation of ϵ

$$\langle \epsilon(x) \epsilon(x+r) \rangle \sim \left(\frac{L}{r} \right)^\mu, \quad (5)$$

where L is a lengthscale of the large structure of the flow. It is evident that the difference between (3) and (4) increases as n increases. In a previous experimental investigation (Antonia, Satyaprakash & Chambers 1982*a*) of velocity structure functions measured in laboratory and atmospheric shear flows, the experimental Reynolds-number variation was compared with predictions of LN and the β -model derived from (2) by setting r equal to the Taylor microscale λ . Both models were found to agree, to within the experimental scatter, with the experimental Reynolds number variation of moments, up to order 6, of the velocity structure function evaluated at $r = \lambda$. Moments of order 8 seemed to be in closer agreement with the β -model than with LN; it was noted, however, that moments of order higher than 8 would be required to validate the β -model. Antonia *et al.* (1982*a*) also plotted inertial-subrange values of moments of order $n+2$ against corresponding values of moments of order n , with a maximum value of n equal to six. On the basis of these plots, it was concluded that LN provided a better representation than the β -model to the power-law behaviour in these plots.

The main purpose of the present paper is to provide data for high-order moments

of the velocity structure functions. Whilst such data have been used to gain a better assessment of LN *vs.* the β -model, it is envisaged that they would eventually be of use in constructing other intermittency models. It was clear that, in the context of LN *vs.* the β -model, or perhaps more generally in the context of deciding between a quadratic and a linear dependence on n of the exponent, that moments of order preferably higher than 8 would be needed. The experimental difficulties associated with the measurement of high-order moments of velocity derivatives have been discussed by Tennekes & Wyngaard (1972) and Frenkiel & Klebanoff (1975). While a decrease in the level of difficulty is expected for obtaining inertial-range structure functions, it seemed nevertheless likely that the experimental uncertainty in defining the tails of the probability density function or the finite dynamic range of the equipment would limit the maximum value of the moment that could be reliably determined. It seems important to know precisely the limitations and to ascertain whether turbulent velocity fluctuations are in fact bounded.

A secondary aim of this paper was to throw further light on the magnitude of the intermittency parameter μ which sets the value of ζ_n for both LN and the β -model. This exponent intervenes in all models that take into account the intermittent nature of the dissipation and quantifies the Reynolds number dependence of the structure functions and velocity derivatives for a given value of n . Antonia, Satyaprakash & Hussain (1982*b*) compared estimates of μ using different statistics of the velocity derivative. Most, although not all, of these statistics indicated a value of μ close to 0.2, instead of a more popular value of 0.5. In the literature, the latter value has usually been inferred from the inertial-subrange behaviour of the spectrum of $(\partial u/\partial t)^2$ ($\equiv \dot{u}^2$ hereinafter).[†] A value of about 0.5 has also been suggested by Chorin (1982) on the basis of a vortex model. Estimates for μ of 0.4 and 0.34 were obtained by Henschel & Procaccia (1982) and Fujisaka & Mori (1979) respectively, using a maximum-entropy principle. It has been pointed out (Nelkin 1981) that the estimate of μ from \dot{u}^2 spectra needs to be carefully interpreted, preferably in the light of the autocorrelation, with inertial-range separations, for \dot{u}^2 . It should also be recalled, however, that a value of $\mu = 0.5$ was obtained by Gagne (1980) from the inertial-range autocorrelations of the centred variable $\dot{u}^2 - \langle \dot{u}^2 \rangle$ (see Gagne & Hopfinger 1979). Autocorrelations for the non-centred variable \dot{u}^2 led to a value of $\mu = 0.2$. Since centred autocorrelations differ only by an additive constant from the non-centred ones, in the asymptotic limit as $R_\lambda \rightarrow \infty$ their power-law behaviour should be the same. As there is no *a priori* reason for using, at moderate Reynolds numbers, a centred instead of a non-centred variable, it seems highly desirable to free the determination of μ from this sort of uncertainty. To this purpose, a brief re-evaluation is made in this paper of estimates of μ obtained from the sixth-order structure functions. It is clear that (3) and (4) yield the same value ($\equiv \mu$) for $\mu_{\frac{1}{3}n}$ when $n = 6$. This result follows from the relation (Frisch *et al.* 1978; Nelkin & Bell 1978)

$$\frac{\langle (\Delta u)^6 \rangle}{r^2} \sim \langle \epsilon(\mathbf{x}) \epsilon(\mathbf{x} + \mathbf{r}) \rangle, \quad (6)$$

where r is the magnitude of the separation vector \mathbf{r} . Frisch *et al.* (1978) conjectured that this relation is model-independent. This conjecture is based on the following relation (e.g. Monin & Yaglom 1975, p. 618):

$$\begin{aligned} \langle \epsilon(\mathbf{x}) \epsilon(\mathbf{x} + \mathbf{r}) \rangle &= \frac{1}{2} \frac{d^2(r^2 \langle \epsilon_r^2 \rangle)}{dr^2} \\ &\sim \langle \epsilon_r^2 \rangle, \end{aligned} \quad (7)$$

[†] It is usually assumed that $\dot{u}^2 \sim \epsilon$.

where ϵ_r is again the dissipation averaged over a volume of dimension r . If we accept (Frisch *et al.* 1978) that velocity differences $\Delta u(r)$ over a volume of size r produce a transfer of energy to smaller scales of the order of

$$\epsilon_r \sim \frac{(\Delta u)^3}{r}, \quad (8)$$

then (6) follows immediately from (8) and (7). The right-hand side of (8) can be interpreted as representing the dissipation of the energy $(\Delta u)^2$ in a time of the order of the eddy turnover time $r/\Delta u$. While (8) leads to the same expression as (1), it is probably worth underlining that (8) expresses a plausible physical idea, whereas (1), which is essentially the point of departure of the modified Kolmogorov (1962) and Obukhov (1962) analyses, is based solely on dimensional analysis. Frisch *et al.* (1978) suggested that careful measurements of the sixth-order structure function would give a useful check on ideas relating energy transfer and energy dissipation. From an experimental point of view, (6) seems to be a useful starting point for determining μ , since it is conjecturably model-independent and sixth-order velocity structure functions can be measured more easily than the dissipation ϵ . Furthermore, (8) tends to suggest that the non-centred dissipation fluctuations are relevant to (6). A few measurements of $\langle(\Delta u)^6\rangle$ in plane and circular jets and the atmospheric surface layer were presented by Antonia *et al.* (1982a). The results were encouraging in that the inertial-subrange behaviour of $\langle(\Delta u)^6\rangle$ indicated a value (≈ 0.2) consistent with the experimentally obtained inertial range behaviour of the autocorrelation of \dot{u}^2 . In the present paper we present further measurements of $\langle(\Delta u)^6\rangle$, paying particular attention to its inertial-range behaviour, in a circular jet and a turbulent duct flow. The reasons for selecting these flows as well as a brief description of the experimental facilities are given in §2, and factors affecting the experimental accuracy of structure functions are considered in §3. In §4 we discuss the inertial-range limits and determine the exponent μ from sixth-order moments and correlations of \dot{u}^2 . The inertial-range behaviour of the structure functions up to order 18 is compared with theoretical models in §5.

2. Flow configurations and instrumentation

2.1. The axisymmetric jet and duct flow

The measurements were made in two different flows: in a fully developed turbulent duct flow and in an axisymmetric jet (Mathieu & Comte-Bellot 1958). The duct had a half-width $b = 9$ cm and an aspect ratio of 12. The hot-wire probe was positioned at a downstream distance $x/b = 59$ and at lateral location $y/b = 0.40$. The present duct is a modified (Maréchal 1970) version of the duct used by Comte-Bellot (1965). Her measurements extended to a maximum downstream distance of $118b$, whereas now the available maximum length is limited to about $60b$. Thus, to enhance the flow establishment, roughness elements were placed at the duct inlet (Gagne 1980). Flow characteristics (table 1) are in general agreement with those measured by Comte-Bellot (1965). Table 1 also contains the conditions for the axisymmetric jet for which structure function measurements were made. The jet nozzle diameter d was 12 cm and the measurement stations were located at $x/d = 25$ and 35. At this distance the flow is not quite self-preserving, but $x/d \leq 35$ was chosen to ensure that the jet development was not influenced by boundary effects. At $x/d = 35$, the outer edge of the jet came close to the floor and a side boundary, but measurements indicated that the turbulence quantities at the centreline remain unaffected. The variations in

Flow	y/b	x/d	U_0^\dagger (m s ⁻¹)	U (m s ⁻¹)	$\langle u^2 \rangle^{1/2}/U$ (%)	λ (mm)	R_λ	η (mm)	η' (mm)	L (cm)	f_K (kHz)	f_c (kHz)
Duct $x/b = 59$	0.4†	—	—	22.40	6.3	5.52	515	0.123	0.106	7.3	33.5	10
	1	—	—	25.62	4.0	4.9	340	0.135	—	—	—	—
Axisymmetric jet	—	25†	15.19	4.12	26.6	7.33	536	0.16	—	17	4.12	7
	—	25	32.04	8.97	24.9	6.02	895	0.10	—	—	—	—
	—	30	31.87	7.21	26.2	6.24	786	0.11	—	—	—	—
	—	35†	31.87	6.32	26.7	7.50	852	0.13	—	24	7.65	—

† Conditions for structure-function measurements. ‡ U_0 is the jet nozzle velocity. § $R_\lambda = \langle u^2 \rangle^{1/2} \lambda / \nu$.

TABLE 1. Characteristics of the fully turbulent duct flow and the axisymmetric jet at the centreline. Lengthscales L , λ and η are respectively the longitudinal integral scale, transverse Taylor microscale $\lambda^2 = U^2 \langle a^2 \rangle / \langle u^2 \rangle$ and the Kolmogorov scale ($\eta = (\nu^2 / 15 U^{-2} \langle \dot{u}^2 \rangle)^{1/2}$, $\eta' = (0.8 \nu^3 / \langle (\Delta u)^2 \rangle)^{1/2}$).

turbulence intensity and Taylor microscale between $25d$ and $35d$ are in agreement with the results of Wygnanski & Fiedler (1969). For comparison, turbulence characteristics at $x/d = 25, 30$ and 35 are shown in table 1 for two different jet velocities. The value of R_λ is practically constant beyond $x/d = 25$ (see also Antonia, Satyaprakash & Hussain 1980), which indicates that the flow is close to self-preservation. At $x/d = 25$ the spatial variation in the total turbulent energy during one turnover timescale is already negligibly small, so that spectral transfers can be considered to be in equilibrium. However, all that is needed for the present purpose is an established inertial subrange, which is not as severe a requirement as an equilibrium spectrum. The duct flow has the advantage of low turbulent intensity ($\lesssim 7\%$), which allows measurements of large negative (relative to the standard deviation σ) fluctuations in velocity by means of hot wires. In a jet, on the other hand, the lower cut-off imposed by the hot-wire anemometer is $(3.5-4)\sigma$. In measurements of high-order structure functions the tails of the probability density function are important, and it is therefore of interest to work in a low-intensity turbulent flow.† This also favours the use of Taylor's hypothesis, which is used in all structure-function measurements reported here.

2.2. Instrumentation

For the structure-function measurements a DISA55M10 constant-temperature system was used together with a standard gold-plated, $5\ \mu\text{m}$ diameter, $1.1\ \text{mm}$ long wire in the jet at $x/d = 25$ and a $3\ \mu\text{m}$ diameter, $0.35\ \text{mm}$ long‡ Wollaston wire at $x/d = 35$ and also in the duct. The latter was also used for measurements of the \dot{u}^2 correlations. The output voltage was first conditioned by subtracting the d.c. component and by low-pass filtering at $50\ \text{kHz}$ (Krohn-Hite filter 3348, at $48\ \text{dB/octave}$) before it was amplified and transmitted on-line to a Preston A/D converter of a Nord 100 computer (see §3). The dynamic range of the whole system was 3×10^4 . When derivatives were required, an analog differentiator, with linear frequency response up to $50\ \text{kHz}$, was used before the line amplifier.

Linearization of the velocity signal was carried out on the computer by fitting a power law to the calibration curve. This is a satisfactory procedure for mean velocities $\gtrsim 30\ \text{cm s}^{-1}$. It was found that, for the jet, linearizations had a drastic effect on the probability density functions, whereas in the duct flow linearization is not essential. No linearization was carried out in the case of velocity-derivative correlation measurements, made in the jet, mainly because large signal excursions, owing to their rare occurrence, contribute little to dissipation correlations, which are moments of fourth order. Besides, linearization, by necessity analog in this case, would have introduced undesirable noise.

3. Accuracy of moments

Tennekes & Wyngaard (1972) concluded that signal-to-noise and integration-time limitations make measurements of moments higher than the fourth of the velocity derivative nearly impossible for signals characterized by a probability density

† The possibility exists that the turbulent velocity fluctuations are bounded in amplitude; this possibility is discussed in §3.2.

‡ In order to reduce averaging effects to a minimum, the ratio of wire length to Kolmogorov scale was kept small as possible ($3 \lesssim l_w/\eta \lesssim 7$) and this at the risk of difficulties which could arise when $l_w/d_w < 200$. The Wollaston wire with $l_w/d_w = 120$, however, gave results consistent with previous measurements made with a wire of $l_w/d_w > 200$ (Gagne 1980).

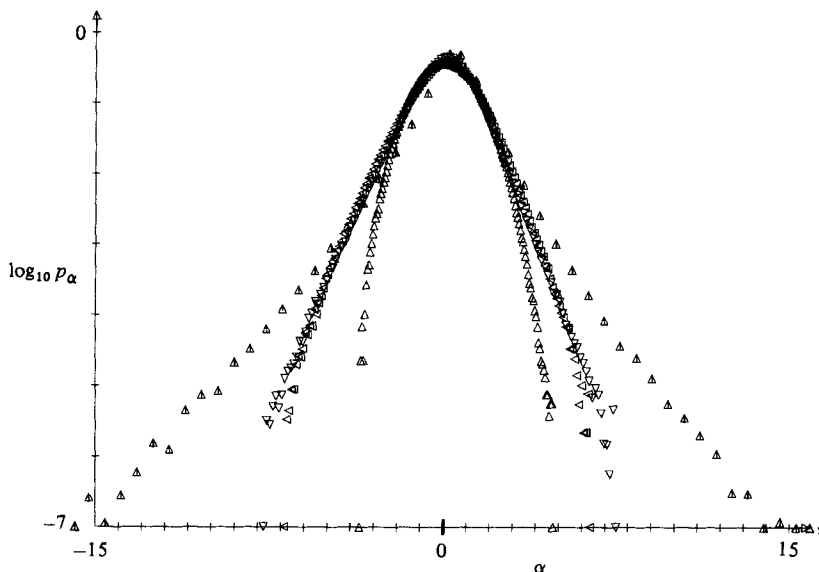


FIGURE 1. Probability density functions in the axisymmetric jet at $R_\lambda = 536$ of u and Δu normalized by their respective standard deviations, $\alpha = \Delta u / \langle \Delta u \rangle^2$: \triangle , $r = 0.6$ mm = 3.5η ; ∇ , 7.7 mm; \triangleleft , 17.2 mm. \triangle , $\alpha = u / \langle u^2 \rangle^{1/2}$.

function with tails extending to large amplitudes of the signal. They considered specifically three possible sources of error, which will be discussed in detail below: the dynamic range of the instrumentation, the resolution of the analog-to-digital converter and the sampling time. In addition, instrumental errors associated with calibration of the hot wire and linearization of the hot-wire response also affect the accuracy of the moments. Repeated calibration showed that the hot-wire response could be represented by a power law to $\pm 1\%$ accuracy (relative to the operation point) for the extreme excursions in velocity. The associated error on the moments was estimated to be about $\pm 20\%$ for the moment of order 12, when it is normalized by the corresponding power of the standard deviation of the function considered, calculated from the same data set. The error is of course not linear in the order of the moment. It is reduced to about $\pm 7\%$ for sixth-order moments and increases rapidly for moments higher than 12. In the jet these high-order moments are however also affected by the erroneous response of the hot wire when the instantaneous velocity becomes nearly zero or negative as a result of large negative excursions in velocity.

The dynamic range of the instrumentation is not a cause for concern in the present experiment since the hot-wire signal was not recorded in analogue form; it was digitized directly using a 14 bit + sign A/D converter (range ± 5.12 V). The dynamic half-range of the converter is about 84 dB ($= 16384$). The maximum number m of standard deviations of Δu that could be recorded in the inertial range was of the order of 30. This should be more than sufficient to enable an accurate estimate of the highest-order moment considered here. The time required to obtain reliable data will be considered in §3.2, while our ability to determine the tails of the probability density function is considered in §3.1.

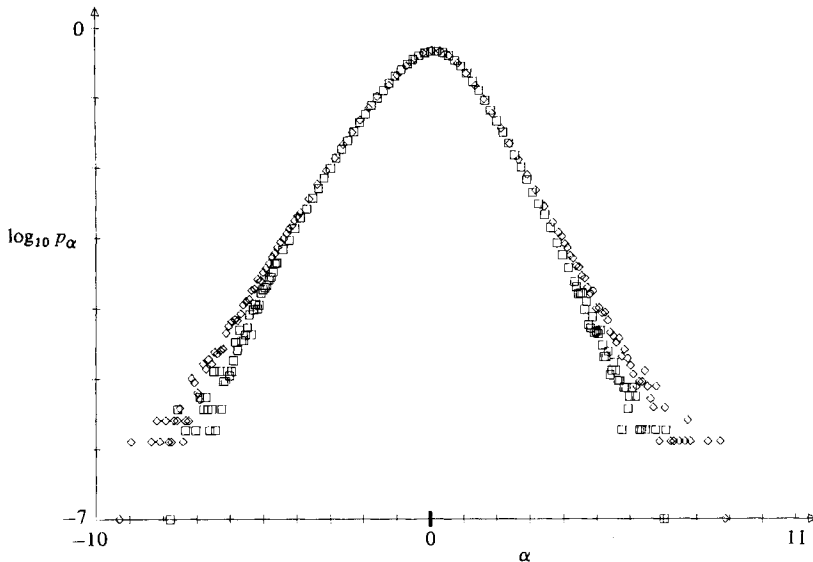


FIGURE 2. Probability density function in the duct flow at $R_\lambda = 515$ of $\alpha = \Delta u / \langle (\Delta u)^2 \rangle^{1/2}$: \diamond , $r = 4.5$ mm; \square , 13.5 mm.

3.1. Probability density functions

The probability density function $p_{\Delta u}$ of Δu is shown in figures 1 (jet) and 2 (duct) for values of r spanning the inertial range (see §4). Also shown in figure 1 is the probability density function of u and of Δu for $r = 3.5\eta$. The latter probability density function is a close approximation to the velocity derivative \dot{u} . The variation of $p_{\Delta u}$ with increasing values of r reflects the same type of behaviour as that described in detail by Van Atta & Park (1972), namely that the most probable value of Δu is found not to be the zero value but rather a small positive value of α . For increasing separations the maximum in the probability density moves to $\alpha = 0$.

It is evident from figure 1 that the difficulties associated with determining $p_{\Delta u}$ are intermediate between those involved in the probability density functions of u and \dot{u} . Tennekes & Wyngaard (1972) emphasized, in the context of measuring the velocity derivative, that data on high-order moments necessitate substantiating evidence in the form of moment distributions. In particular, moments α^n of a signal α cannot be trusted if the integrands $\alpha^n p_\alpha$, which feature in the defining relation

$$\langle \alpha^n \rangle = \int_{-\infty}^{\infty} \alpha^n p_\alpha d\alpha,$$

have not decreased at the largest values of α measured, to a level at which the integral can be computed with reasonable accuracy. The probability density function of Δu ($\alpha = \Delta u / \langle (\Delta u)^2 \rangle^{1/2}$) is shown in figure 3 for $r \approx \lambda$ on a log-linear plot. The experimental data only extend to $|\alpha| \approx 9$, but for $|\alpha| \gtrsim 2$ the solid straight lines are adequate fits to the data. Similar fits were obtained for probability density functions obtained at other inertial subrange separations for r . These straight lines suggest an exponential form for the probability density function; this form has already been noted by Tennekes & Wyngaard (1972) and Frenkiel & Klebanoff (1975) in connection with the velocity derivative. These authors extrapolated this form to large values of α in an attempt to obtain correct estimates for $\langle \alpha^n \rangle$. Tennekes & Wyngaard underlined, however, the uncertainty that the experimental data would follow the extrapolation of this exponential probability density function to extreme values of α .

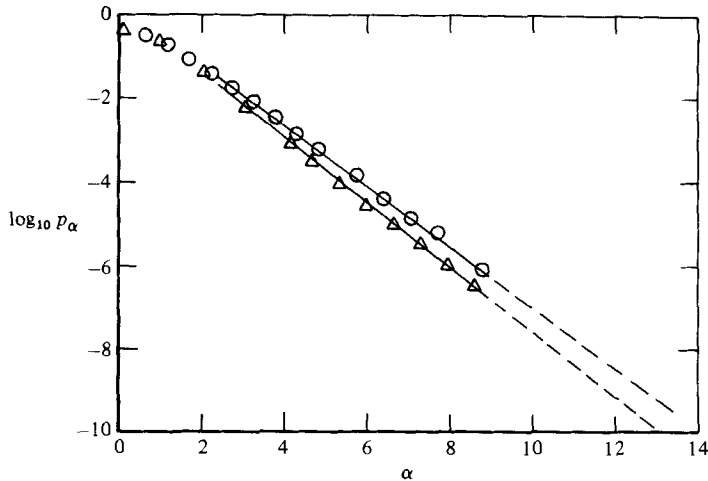


FIGURE 3. Probability density function of $\Delta u / \langle (\Delta u)^2 \rangle^{1/2}$ for $r \approx \lambda$ in axisymmetric jet at $R_\lambda = 536$: \circ , $\alpha = \Delta u / \langle (\Delta u)^2 \rangle^{1/2} < 0$; \triangle , $\alpha > 0$. Broken lines are extrapolations of solid lines beyond the experimental range of α .

The integrand $\alpha^n p_\alpha$ is shown in figure 4 for $n = 12$ and for both positive and negative values of α . The closure of the integrand is achieved only by using the exponential extrapolation of p_α ; the parts of the integrand deduced from this extrapolation are shown as broken curves on figure 4. The large value of n highlights the significant contribution made by the negative part of the probability density function to $\langle \alpha^n \rangle$. The value of $\langle \alpha^n \rangle$ computed directly† from the digital time series is 30% smaller than that inferred from the extrapolated integrand in figure 4. The difference between extrapolated and non-extrapolated values clearly decreases as the order of the moment decreases. An important observation, however, is that there was no significant variation of this difference as the separation r changes in the inertial subrange. The implication of this observation with regard to the results of §5 is that the inertial-subrange power-law exponents could be correctly obtained from the $\langle (\Delta u)^n \rangle$ data inferred using the non-extrapolated probability density functions. The maximum value of n for which this can be done is not known but for the present conditions (§5) $n = 14$ seems reliable, whereas $n = 16$ or 18 may be suspect because of oscillations exhibited by these structure functions.

To improve the accuracy in determining the integrand $\alpha^n p_\alpha$, when $\alpha \equiv \dot{u}$, Frenkiel & Klebanoff used an interpolation procedure consisting of dividing the intervals between digitized points into steps corresponding to consecutive integer values within each interval. This procedure led to a significant increase in the number of individual data points and reduced the scatter in the measured tails p_α , thus permitting a more reliable extrapolation of p_α . This interpolation procedure was not implemented here partly because the scatter in the tails of p_α would be smaller for $\alpha \sim \Delta u$ than $\alpha \sim \dot{u}$, but mainly because the interpolation introduces a bias which needs to be estimated accurately. It should be noted, however, that the extrapolation of the 'smoothed' interpolated data of Frenkiel & Klebanoff also follows the exponential form.

An interesting question that arises is whether the experimental probability density function will continue to decrease to extremely large values of α or whether the signal α will in fact be bounded. The last proposition is difficult to test in view of the decreasing frequency at which increasing values of α occur. Tennekes & Wyngaard

† This value was in close agreement with that inferred from the non-extrapolated probability density function.

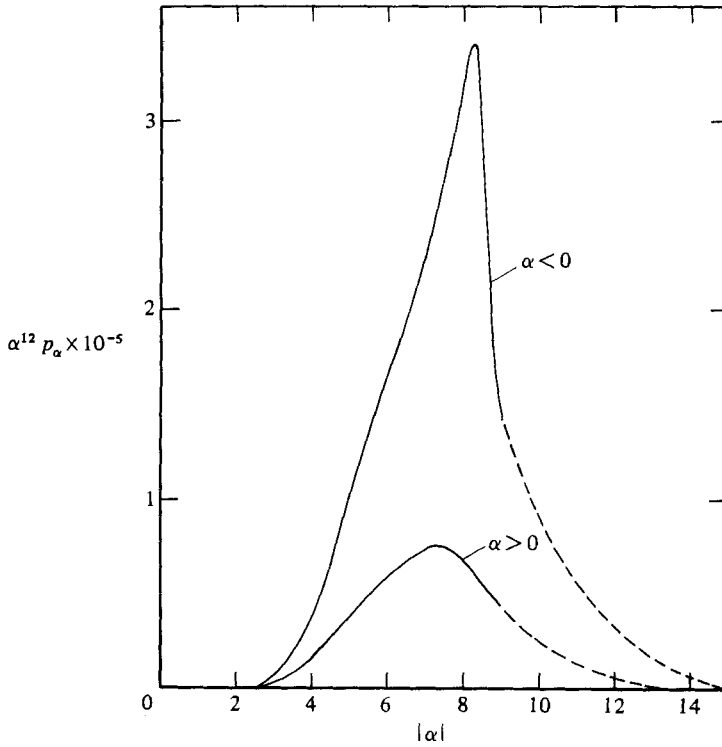


FIGURE 4. Probability density function of Δu multiplied by Δu^{12} for $r \approx \lambda$ in axisymmetric jet at $R_\lambda = 536$. Broken lines are extrapolations of solid lines beyond the experimental range of α .

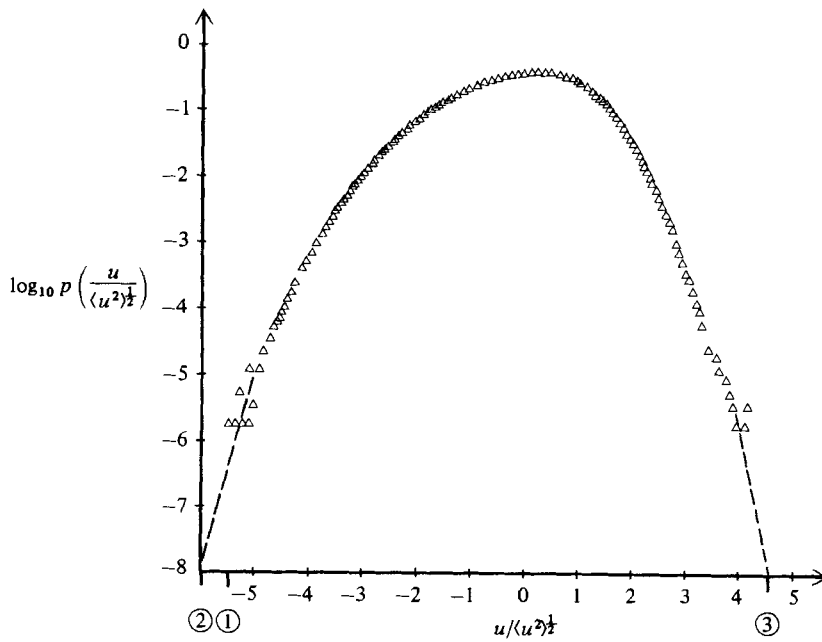


FIGURE 5. Probability density function of u in the duct flow showing an exponential extrapolation to 10^{-8} and the limits set by electronic counters. No excursions exceeded limits 2 and 3.

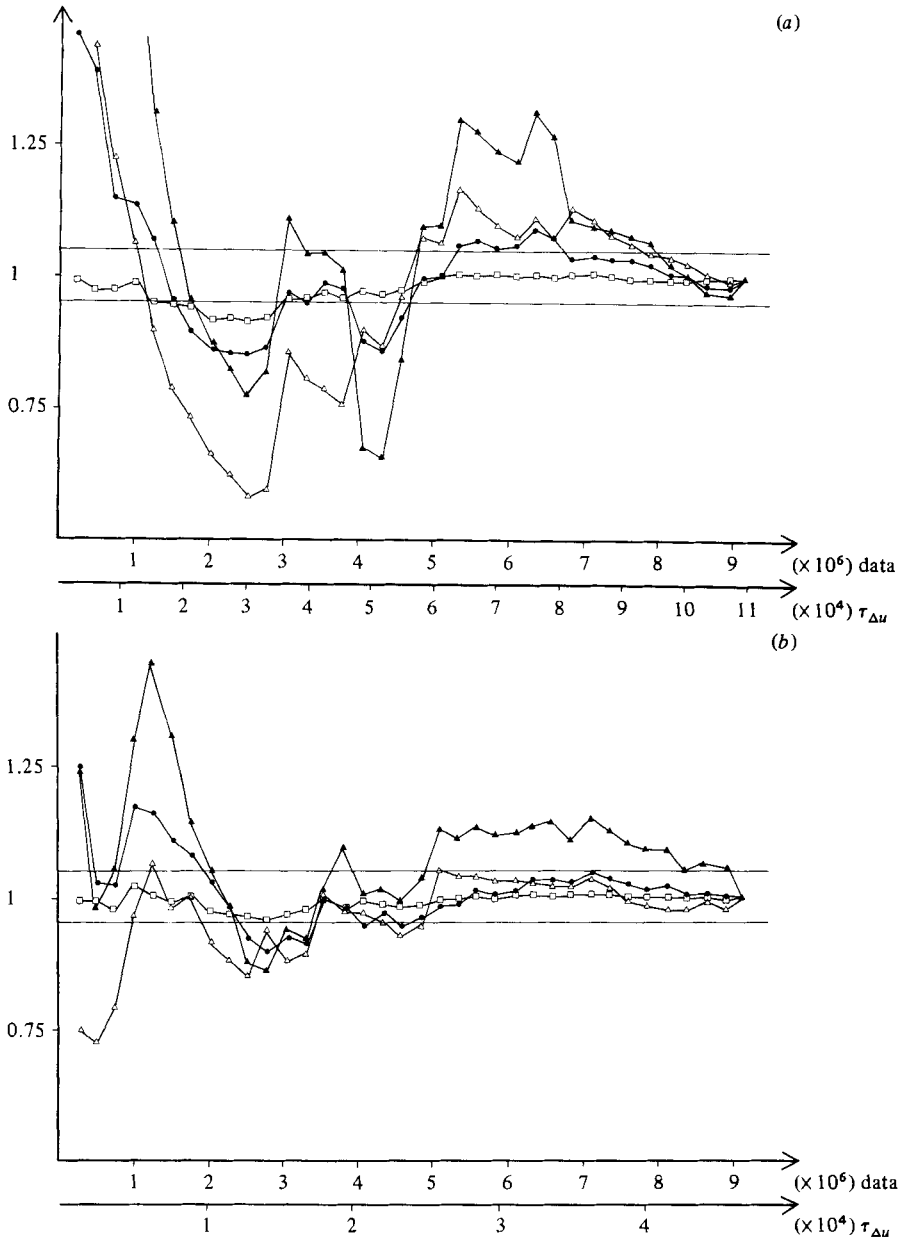


FIGURE 6. Convergence in time of structure functions to their value obtained from maximum record length, for two values of r corresponding to the inertial-range limits in the jet at $R_\lambda = 536$. (a) $r = 4.6 \text{ mm} = 29\eta$: \square , $n = 6$; \bullet , 7 ; \blacktriangle , 11 ; \triangle , 12 . $\tau_{\Delta u} = 11.7 \text{ ms}$ ($\tau_{\Delta u}$ is the turnover time $r/\Delta u$). (b) $r = 17.6 \text{ mm} = 110\eta$, with same symbols as in (a). $\tau_{\Delta u} = 27.2 \text{ ms}$.

noted that the number of excursions of \dot{u} beyond $20\langle\dot{u}^2\rangle^{\frac{1}{2}}$ were too small, even after several hours of recording time, to lead to a statistically stable average. The frequency of occurrence of large values of u was examined here for the duct flow with the hot wire at $y/b = 0.4$. The signal was compared with comparator levels set at $-5.5\langle u^2\rangle^{\frac{1}{2}}$ and $-6\langle u^2\rangle^{\frac{1}{2}}$, and the number of times these levels were exceeded was registered by electronic counters. For a $2\frac{1}{2}$ h period, only 20 counts were found at $-5.5\langle u^2\rangle^{\frac{1}{2}}$, with no counts for $-6\langle u^2\rangle^{\frac{1}{2}}$. On the positive side, no excursions exceeded $+4.5\langle u^2\rangle^{\frac{1}{2}}$ over a 3 h period. This duration should be compared with the 20 min record time

corresponding to 9.2×10^6 samples, the maximum available disc capacity. In figure 5 we show the probability density function of u in the duct flow with an exponential extrapolation to 10^{-8} , an expectation corresponding to a record duration of $2\frac{1}{2}$ to 3 h. The limits set by the counters are also indicated. This figure shows that the probability density function seems to fall off more rapidly than the exponential rate. In any case, these observations highlight the futility of extending the duration of the digital record. This was also supported by observation in the jet. In this flow, negative excursions are, in this case, already limited to about 3.5σ by the hot-wire response.

3.2. Convergence time

Two different criteria for determining the time required to obtain reliable data on moments have been considered. First, the time required for convergence of a moment to within $\pm 5\%$ of its final value has been determined from running averages of $(\Delta u)^n$, such as shown in figure 6 for two values of r corresponding to the inertial-subrange limits and for both even and odd values of n ranging from 6 to 12. In figure 6 the running averages have been normalized by the final values attained at the end of the full digital record.

A number of observations can be made.

(i) Even and odd moments exhibit a number of oscillations whose amplitude generally decreases with time.

(ii) Fluctuations are usually approximately in phase for both even and odd moments. However, even and odd moments are occasionally out of phase for some separations.

(iii) Convergence for the larger separations is more rapid.

Convergence is here considered to be attained when the moments oscillate within the $\pm 5\%$ limits over one or more oscillation periods. For large separations this is satisfied for all moments $n \leq 12$, whereas, for small separations, this criterion is not fulfilled for the higher-order moments.

Five per cent convergence times inferred from figure 6 are plotted in figure 7. Times for odd moments are generally larger than those for adjacent even moments; this supports the trend previously established (e.g. Antonia & Van Atta 1978; Antonia *et al.* 1982*a*) for both velocity and temperature structure functions. It should be noted that the overall record time is larger than the longest time required for convergence (in the present case for $n = 11$). Also note that, for even moments, the convergence time decreases, on average, as r increases. This trend is not apparent for odd moments: there is, perhaps surprisingly, relatively little variation of the odd moments over the inertial subrange.

The mean-square relative error involved in computing the mean values of a stationary quantity α^n can be approximated (Tennekes & Lumley 1972) by $2[(F_{2n}/F_n^2) - 1] I_n/T$, where $F_{2n} = \langle \alpha^{2n} \rangle / \langle \alpha^2 \rangle^n$, $F_n = \langle \alpha^n \rangle / \langle \alpha^2 \rangle^{\frac{1}{2}n}$, I_n is the integral timescale of α^n and T is the finite integration time, assumed to be much greater than I . When α is replaced by the velocity difference Δu , the integral timescale can be defined as

$$I_1 = \int_0^\infty \frac{\langle [u(t+\tau) - u(t)][u(t'+\tau) - u(t')] \rangle}{\langle (\Delta u)^2 \rangle} d\tau_1, \quad (9)$$

where $t' = t + \tau_1$. I_1 can be rewritten in terms of the correlation coefficient ρ of u as

$$I_1 = \frac{\langle u^2 \rangle}{\langle (\Delta u)^2 \rangle} \int_0^\infty [2\rho(\tau_1) - \rho(\tau_1 - \tau) - \rho(\tau_1 + \tau)] d\tau_1. \quad (10)$$

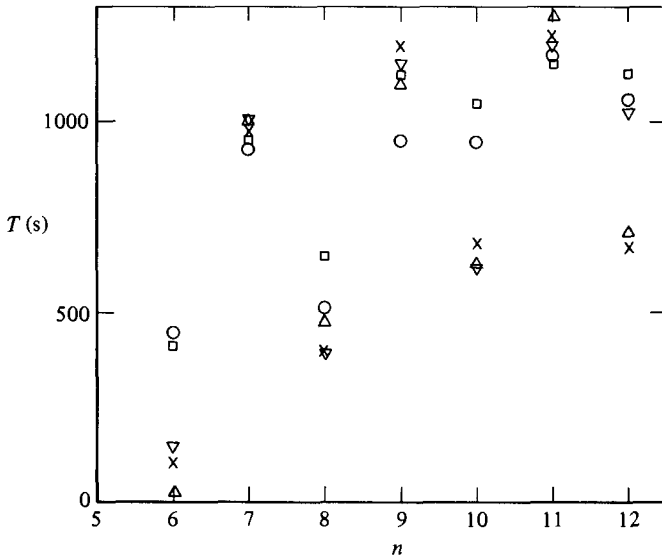


FIGURE 7. Time for moments of order n of Δu to reach $\pm 5\%$ of their final value. Record duration is 22 min. \square , $r/\eta = 29$; \circ , 48; ∇ , 62.5; \triangle , 110; \times , 184.

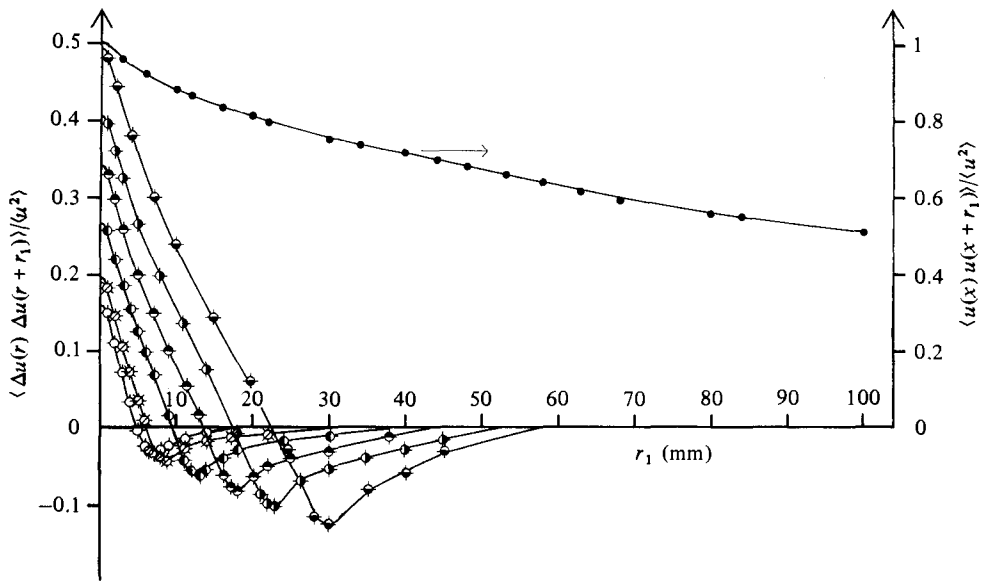


FIGURE 8. Autocorrelation functions of u and of Δu , normalized by $\langle u^2 \rangle$ in the jet at $R_\lambda = 536$. The values of r for $\Delta u(r)$ are \circ , $r = 6$ mm; \otimes , 7.7; \bullet , 12; \ominus , 17; \oplus , 22; \odot , 29.5. The autocorrelation $\langle \Delta u(r) \Delta u(r+r_1) \rangle / \langle u^2 \rangle$ corresponds to the integrand (10).

The integrand can be obtained, relatively economically, from a knowledge of the correlation coefficient $\rho(\tau_1)$. The latter can be inferred from the second-order structure function, viz

$$\rho(\tau_1) = 1 - \frac{1}{2} \frac{\langle [\Delta u(\tau_1)]^2 \rangle}{\langle u^2 \rangle}. \tag{11}$$

There is some advantage in determining ρ indirectly via the second-order structure function rather than by correlating time-delayed velocity signals, either directly or

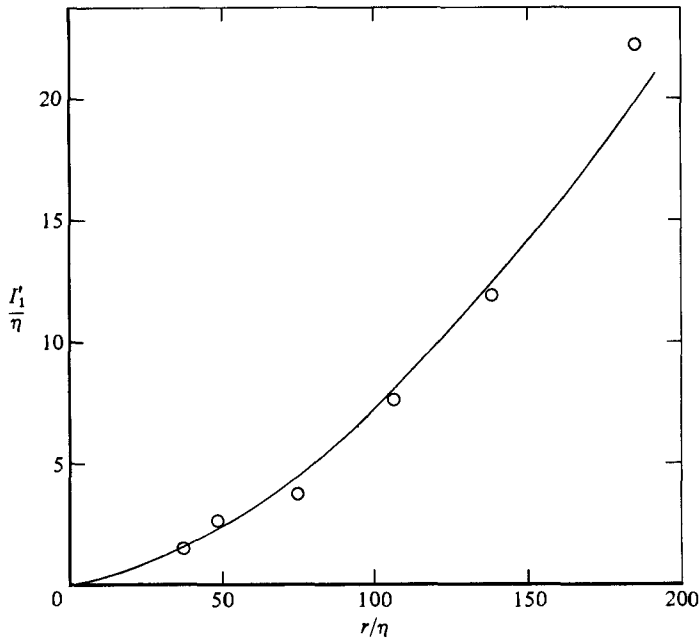


FIGURE 9. Variation of integral lengthscale of Δu , normalized by the Kolmogorov scale η , with r/η . Solid curve is least-squares fit $4.13 \times 10^{-3}(r/\eta)^{1.625}$.

by inverse-Fourier-transforming the velocity power spectrum. While the reliable direct determination of ρ may be rendered difficult by the presence of low-frequency fluctuations, the second-order structure function does not, in fact, contain frequencies below a certain limit, proportional to (nominally) τ^{-1} (Gagne 1980). An illustration of this behaviour is provided by the distributions (figure 8) of the integrand in (10). Also shown in figure 8 is the distribution of $\rho(\tau_1)$, plotted on a different scale, which was determined using (11) and which led to the determination of the integrand. As $\tau \rightarrow 0$, the positive and negative contributions to the integrand become more equal; this conforms with the expectation of a zero integral timescale for the time derivative of the velocity signal. An interesting observation is that the location of the minimum value of the integrand is very approximately equal to τ or, when converted to length as in figure 8, to r ($\equiv -U\tau$). The integral lengthscale I'_1 ($\equiv I_1 U$) derived from the distributions of figure 8 increases with increasing r from zero, the value appropriate to \dot{u} , to that corresponding to the integral scale of u . The solid curve in figure 9 is a least-squares power-law fit to the data. The increase of I'_1/η with r/η is qualitatively similar to the increase reported by Antonia & Van Atta (1978) for integral timescales associated with temperature structure functions. Estimates of mean-square errors of moments of order n can only be made if integral timescales associated with these moments are known and if moments of order $2n$ are available. For $n = 2$ a reasonable estimate of the integral timescale would be about $0.6I_1$ (Sreenivasan, Chambers & Antonia 1978; Antonia & Van Atta 1978). In the jet, at $r \approx \lambda$, the flatness factor of Δu is about 4.4 and the r.m.s. error for the present record duration (1310 s) is about 0.05%. In the case $n = 6$, with measured values of $\langle(\Delta u)^{12}\rangle/\langle(\Delta u^2)\rangle^6$ and $\langle(\Delta u^6)\rangle/\langle(\Delta u^2)\rangle^3$ equal to 1.05×10^6 and 44.6 respectively and with a conservative 'guess' for the timescale equal to $0.4I_1$, the r.m.s. error is about 0.4%. Using the Lumley-Tennekes formula, the record duration required to obtain $\langle(\Delta u)^6\rangle$ to an

r.m.s. error of 5% is about 23 s. In contrast, the time required for the running moment of $(\Delta u)^6$ to converge to within $\pm 5\%$ of the final mean is 410 s (figure 7). However, it should be noted (Antonia & Van Atta 1978) that no direct correspondence has been established between the convergence time, as inferred from figure 6, and the time required to achieve a stationary mean for a prescribed mean-square relative error. In view of the uncertainty involved in estimating higher-order moments of Δu and their integral scales, the estimates of figure 6 may provide a better guide for experimental record durations than the application of the Tennekes–Lumley formula.

4. Determination of the constant μ

The behaviour of the structure function of order 6 seems best suited for the determination of μ through the use of (6) and (5). Structure functions are not as prone to experimental uncertainty as are dissipation correlation measurements. The principal source of error in determining μ stems from the definition of the limits of the inertial range. Usually the inertial range is determined from second-order moments (or the spectral equivalent) but it must be realized that second-order moments are subject to (weak) intermittency corrections. The third-order moments

$$\langle(\Delta u)^3\rangle = -C_3 r \langle\epsilon\rangle,$$

on the other hand, are free of any intermittency assumptions, and the constant C_3 is known ($= \frac{2}{3}$) for locally isotropic turbulence.

4.1. Inertial-range limits

In figures 10(a, b) the normalized second-, third- and sixth-order weighted structure functions

$$\frac{\langle(\Delta u)^n\rangle}{V_K^n} \left(\frac{r}{\eta}\right)^{-\zeta_n} = C_n \quad (n = 2, 3, 6), \quad (12)$$

where $C_n = -C_n^* \eta^{-\mu_n}$ are constants† and $V_K = (\nu \langle\epsilon\rangle)^{\frac{1}{2}}$ and $\eta = (\nu^3 / \langle\epsilon\rangle)^{\frac{1}{4}}$ are respectively the Kolmogorov velocity and lengthscales, are plotted logarithmically as functions of r/η . This normalized representation highlights more clearly the existence of a plateau characteristic of the inertial range. It is seen from figure 10(a) that, for the jet with $R_\lambda = 536$ (table 1), the third-order structure function weighted by r/η has a true plateau in the range $35 \lesssim r/\eta \lesssim 80$. It is, however, reasonable to extend the inertial range to $25 \lesssim r/\eta \lesssim 105$, over which the experimental points show only a small deviation (about 1%) from this plateau. For conditions corresponding to $R_\lambda = 852$ shown in figure 10(b) the inertial range of $\langle(\Delta u)^3\rangle$ is $20 \lesssim r/\eta \lesssim 150$.

On the other hand, the data for $\langle(\Delta u)^2\rangle$ in figures 10(a, b) indicate a wider inertial range, when the ratio $\langle(\Delta u)^2\rangle / V_K^2$ is multiplied by $(r/\eta)^{-\frac{2}{3}}$ ($60 \lesssim r/\eta \lesssim 200$ for $R_\lambda = 536$ and $50 \lesssim r/\eta \lesssim 500$ for $R_\lambda = 852$). In this context it should perhaps be noted that the data of Van Atta & Chen (1970), obtained in the boundary layer over the ocean, also suggest that the inertial range, as inferred from $\langle(\Delta u)^3\rangle$, is narrower than that deduced from $\langle(\Delta u)^2\rangle$. These authors noted that, for the narrower inertial range, 0.72 is a considerably better fit to the data than $\frac{2}{3}$. On the other hand, the axisymmetric-jet data ($R_\lambda \approx 1000$) presented in Antonia *et al.* (1982a) suggested approximately identical inertial ranges of approximately one decade in extent, associated with either second- or third-order structure functions. All moments of Δu should indeed exhibit the same

† C_n^* are the Kolmogorov ‘41’ constants, i.e. those that pertain to no intermittency ($\mu = 0$).

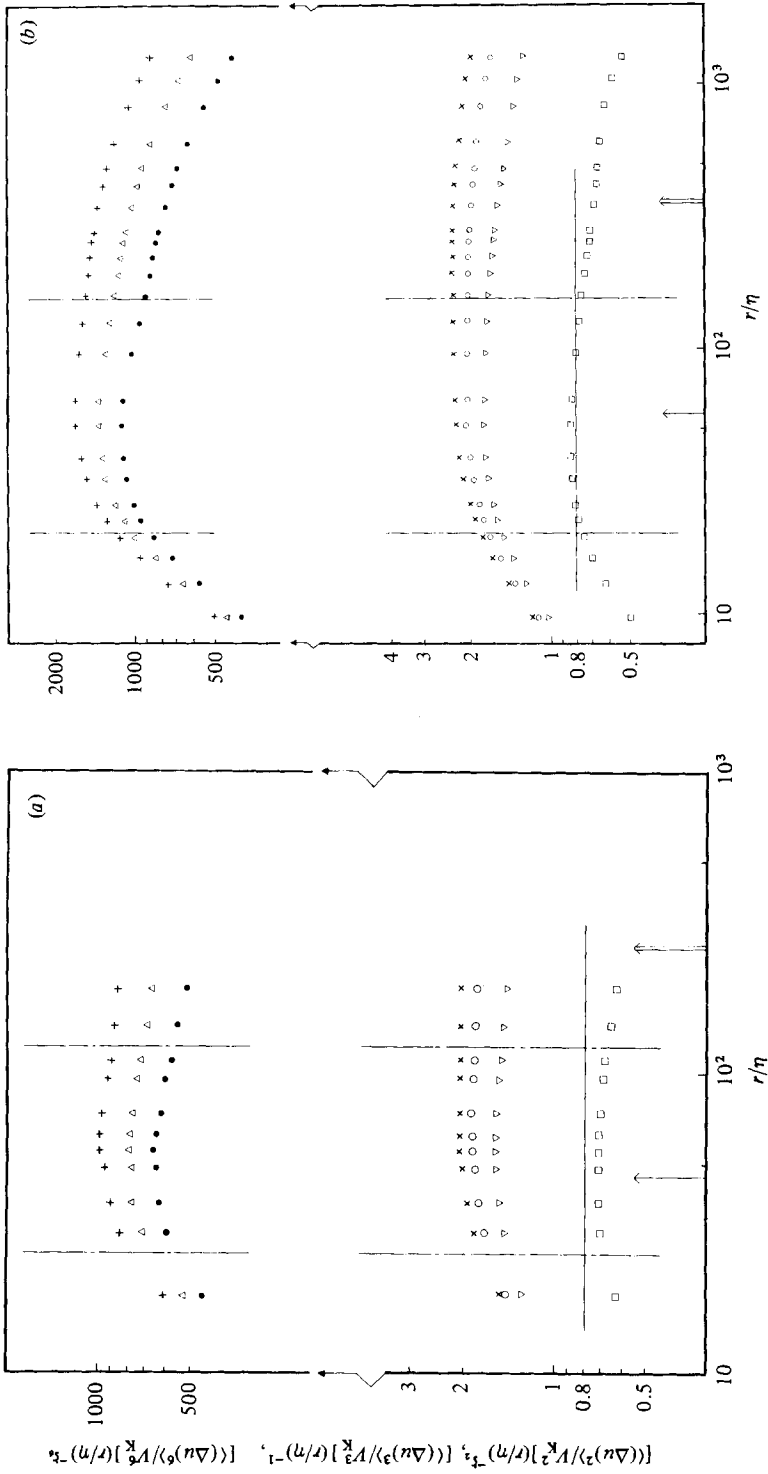


FIGURE 10. Structure functions of second-, third- and sixth-order multiplied by appropriate powers of r/η , with r/η in the jet: \square , $[\langle(\Delta u)^3\rangle/V_K^3] (r/\eta)^{-1}$; \times , $[\langle(\Delta u)^2\rangle/V_K^2] (r/\eta)^{-2}$; \circ , $(r/\eta)^{-0.89}$ (LN with $\mu = 0.2$); ∇ , $(r/\eta)^{-0.73}$ (β -model, $\mu = 0.2$); $+$, $[\langle(\Delta u)^6\rangle/V_K^6] (r/\eta)^{-1.75}$; \triangle , $(r/\eta)^{-1.85}$; \bullet , $(r/\eta)^{-1.8}$; \odot , $(r/\eta)^{-1.85}$. (a) $R_\lambda = 536$. (b) $R_\lambda = 852$. The vertical lines $- \cdot - \cdot -$ indicate the inertial-range limits, the vertical arrow the Taylor microscale, and the double vertical arrow indicates $\frac{1}{2}L$.

universal subrange. In practice it may be difficult to decide on the extent of the inertial range for an arbitrary order n of the moment, since the corrections to the power-law exponents in Kolmogorov's (1941) original theory are not known *a priori*. There is little doubt that the customary determination of the inertial range has been via the use of $n = 2$ (the lowest non-trivial order), partly because of the availability, in relatively reliable form, of $\langle(\Delta u)^2\rangle$ and partly because of the often-expressed view that deviations from the $\frac{2}{3}$ exponent for $\langle(\Delta u)^2\rangle$ are too small to be detected reliably. This latter view is perhaps arguable since, in the case of the β -model, the exponent is as large as 0.73 with $\mu = 0.2$. The importance of the effect of intermittency on the second order power-law exponent is clearly seen from figures 10(*a*, *b*), which also contain the second-order structure functions corrected respectively by the LN and β -model with $\mu = 0.2$ (LN: $\xi_2 = \frac{2}{3} + 0.0222$; β -model: $\xi_2 = \frac{2}{3} + 0.0666$ for $\mu = 0.2$). The correction has two effects: one is to make the inertial range somewhat narrower, and the other, more important, effect is to shift the inertial range to lower values of r/η , making it coincide with the $\langle(\Delta u)^3\rangle$ inertial range. The data suggest a correction intermediately between LN and the β -model. It may be noted that the correction also lowers the constant C_2 by about 10% to $C_2 \approx 1.95$ for an exponent of 0.7.

Figure 11 shows the second-, third- and sixth-order structure functions in the form (12) for the duct corresponding to $R_\lambda = 515$ (table 1). In this case the third-order structure function would suggest an inertial range extending to $r/\eta \approx 300$;† the second-order (corrected) moments set, however, a more plausible upper limit of $r/\eta \approx 110$, so that the inertial range can be taken as $30 \lesssim r/\eta \lesssim 110$.

While the convergence rate of third-order moments is slower than for second-order moments, the use of $\langle(\Delta u)^3\rangle$ should, in the context of locating the inertial range, be preferred to $\langle(\Delta u)^2\rangle$ in view of the unambiguity in the power-law exponent for $\langle(\Delta u)^3\rangle$ in relation to that for $\langle(\Delta u)^2\rangle$. The duct-flow data suggest, however, that it is best to look for a concordance in both the $\langle(\Delta u)^3\rangle$ range and the corrected $\langle(\Delta u)^2\rangle$ range. Furthermore, the point $r = \lambda$ should fall within the inertial range.

An aspect of importance for calculating the Kolmogorov scales used in (12) is the assumption of local isotropy when $\langle\epsilon\rangle$ is calculated from $\langle\epsilon\rangle = 15\nu U^{-2} \langle\dot{u}^2\rangle$. A possible criterion of isotropy for scales contributing to \dot{u} may be the degree to which the experimental value of C_3 approximates to $\frac{4}{5}$. For the jet the third-order structure functions give values of 0.70 and 0.80 for $R_\lambda = 536$ and 852 respectively when $\langle\epsilon\rangle$ is calculated using the isotropic relation. These values indicate that local isotropy is well approximated in the jet, especially if we allow for the experimental uncertainty in determining \dot{u} . In the duct, at $y/b = 0.4$, local isotropy seems tenuous in view of the value 1.4 for C_3 when the isotropic value of $\langle\epsilon\rangle$ is used. In order to verify whether it is indeed a lack of isotropy which is at the origin of this rather large value of C_3 , we measured third-order structure functions at the duct centreline, where an approach to isotropy is expected. It was found that C_3 was indeed closer to the isotropic value $\frac{4}{5}$ (≈ 1.0 at the duct centreline). Measured turbulent fluctuations at the jet and duct centrelines indicated that isotropy is better approximated for the jet than for the duct, which seems consistent with the difference in the C_3 values.

Two estimates of the Kolmogorov microscale are given in table 1 for the duct flow; namely η calculated using an isotropic $\langle\epsilon\rangle$, and η' calculated using $\langle\epsilon\rangle$ inferred from the third-order structure functions with $C_3 = \frac{4}{5}$. When η' is used in (12), a value of 0.55 is obtained for the Kolmogorov constant $C_2/4.02$ using second-order structure functions (using a $\frac{2}{3}$ power law). Note that η' was used as the normalizing lengthscale. The effect of this is to shift the inertial range to higher values of r/η' than in the case

† The extent of the $\langle(\Delta u)^3\rangle$ inertial range is considered further later in this section.

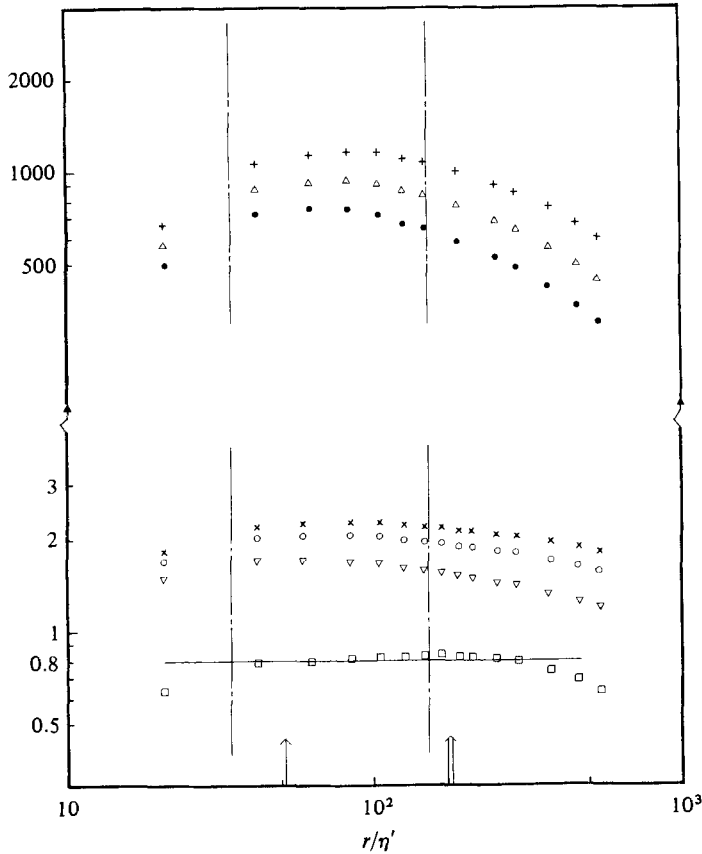


FIGURE 11. Structure functions of second-, third- and sixth-order multiplied by appropriate powers of r/η' , with r/η' in the duct flow at $R_\lambda = 515$. Symbols and ordinate as for figure 10 (all values calculated with η').

of the jet for practically the same value of R_λ . The use of η' does, however, make the constants C_n (the agreement for C_3 is forced) agree with those of the jet for all the values of n considered.

4.2. The value of the constant μ

Sixth-order structure functions give direct access to the constant μ . In figures 10(a, b) and 11 these have been presented together with $\langle(\Delta u)^2\rangle$ and $\langle(\Delta u)^3\rangle$ to allow a proper assessment of the inertial-range behaviour. The sixth-order moments have been weighted by three different values of the exponent ζ_6 which is related to μ by $\mu = 2 - \zeta_6$. An examination of the three different cases shown in figures 10(a, b) and 11 suggests that $1.75 \leq \zeta_6 \leq 1.85$, the mid-range value of 1.8 yielding a value of 0.2 for μ . From the behaviour of the sixth-order moments it is clear that a shift in the inertial-range limits to larger values of r/η would increase the value of μ , whereas a shift to lower values would cause a decrease in μ . For instance, a value of $\mu = 0.35$ would be appropriate in the range $60 \lesssim r/\eta \lesssim 200$ inferred from a $\frac{2}{3}$ law for $\langle(\Delta u)^2\rangle$. Compared with the duct, the upper limit of the jet inertial range could be somewhat increased, but $\mu = 0.2 \pm 0.05$ continues to be the best estimate of the sixth-order structure function inertial-range behaviour.

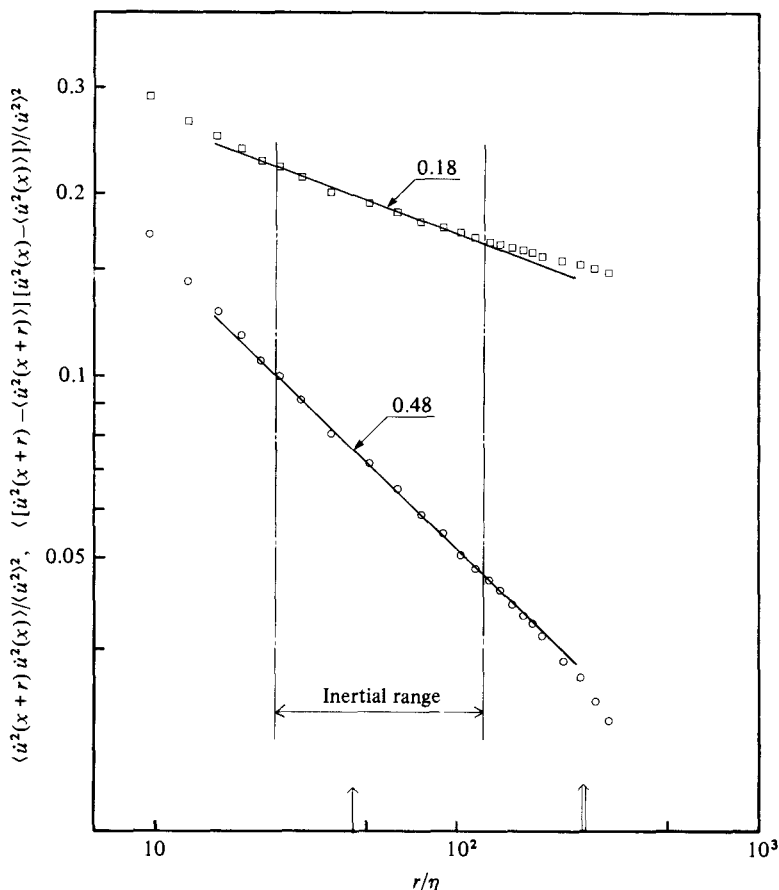


FIGURE 12. Correlations of \dot{u}^2 and $\dot{u}^2 - \langle \dot{u}^2 \rangle$ normalized by $\langle \dot{u}^2 \rangle$, with r/η in the jet at $R_\lambda = 536$. The inertial range determined from figure 10(a) is indicated by vertical chain-dotted lines. The slopes that fit the data in the inertial range are also indicated. \square , \dot{u}^2 ; \circ , $\dot{u}^2 - \langle \dot{u}^2 \rangle$.

This value of μ is in remarkably good agreement with the value obtained by Antonia *et al.* (1982*b*) from correlations of \dot{u}^2 and by Frenkiel & Klebanoff (1975) from the asymptotic relation for the variance of $\ln \epsilon_r$. However, as discussed by Antonia *et al.* (1982*b*), these latter procedures are based on several questionable assumptions. It should be noted that the assumption that the instantaneous dissipation ϵ is proportional to $\nu U^{-2} \dot{u}^2$ seems plausible in the sense that the degree of anisotropy is likely to vary only little over the inertial range. On the other hand, the setting of the cut-off frequency can be problematic, especially at large R_λ , when derivatives are used. As noted previously, structure functions are less subject to arbitrary assumptions and the results obtained substantiate the value of 0.2 for μ .

It was pointed out in §1 that this value is not in contradiction with $\mu \approx 0.5$ usually inferred from the inertial-range behaviour of the ϵ -spectrum, which is equivalent to considering centred moments of ϵ . The correlations of fluctuations of \dot{u}^2 with respect to $\langle \dot{u}^2 \rangle$ indeed yield $\mu \approx 0.5$ (Gagne & Hopfinger 1979), consistent with $\mu \approx 0.2$ obtained for the correlation of the non-centred fluctuation \dot{u}^2 . To demonstrate this more decisively, we have plotted in figure 12 the correlations of \dot{u}^2 and $\dot{u}^2 - \langle \dot{u}^2 \rangle$ measured in the jet, $R_\lambda = 536$. The inertial range limits obtained from figure 10(a) are indicated,

and the slope was determined in this range. The values of the exponents which give the best fits to the data are respectively $\mu = 0.18$ and $\mu_c = 0.48$. It is worth noting, however, that earlier available measurements of $\langle(\Delta u)^6\rangle$ do not support the present value of $\zeta_6 = 1.8$. The data of Van Atta & Park (1972) indicate a value of 1.5. Mestayer's (1980) data indicated a $\langle(\Delta u)^2\rangle$ inertial range of almost one decade in extent. For this range, the data for $\langle(\Delta u)^6\rangle$ indicated a value of 1.65 for ζ_6 . It should be noted, however, that the $\langle(\Delta u)^3\rangle$ data exhibit a bump at $r \approx \lambda$ and the resulting inertial subrange would be significantly narrower than that inferred from $\langle(\Delta u)^2\rangle$. A value of 1.8 is possible over a reduced range of r . The sampling frequency used by Mestayer was also rather low (the lower cut-off corresponds to the lower inertial-range limit), which results in poor resolution of the lower end of the inertial range.

With regard to Van Atta & Park's results, satisfactory convergence of the probability density functions was indicated *only* for their largest values of r (their inertial range was almost three decades in extent). For small r and $n \geq 5$ they indicated that the maxima in the probability density function integrands may not be reached and that their moments would be suspect. The total number of samples in their experiment was one order of magnitude smaller than that in the present experiment. Figure 7 indicates that for convergence of the sixth-order structure function about 3×10^6 data points are needed at small separations when $R_\lambda \lesssim 500$. Van Atta & Park only used 6×10^5 samples at $R_\lambda \approx 3000$. We have examined structure functions obtained from both our complete data set and from only part of it. When the number of samples is smaller by a factor of 2–3 than that required for convergence, the slope is not changed by a noticeable amount, although the value of the moment is quite different. However, when the factor is increased to about 10, the calculated structure functions show considerable oscillations, which can lead to incorrect estimates of the power-law exponents.

5. High-order structure functions

In this section the inertial-range behaviour of high-order structure functions is examined with a view to assessing different intermittency models. For μ we use the value of 0.2, determined in §4.

5.1. Structure functions up to order 18

The LN model predicts a decreasing inertial-range slope when the order $n > 3(\mu + 2)/2\mu$; in contrast, the β -model suggests a slope that increases linearly with n . It is clearly desirable to measure structure functions for values of n beyond that, n^* say, for which change of sign is expected to occur in the rate of change of the slope in the LN model. With $\mu = 0.2$, n^* is about 16. Unfortunately, for reasons given in §3, the probability density function is reasonably well defined only up to order 12. This nonetheless represents significant progress compared with available data (Van Atta & Park 1972; Gagne & Hopfinger 1979; Mestayer 1980). In view of the weak effect non-convergence has on the slope (see §3 and the end of §4) we believe that the duct data for $n = 14$ and the jet ($R_\lambda = 852$) data for $n = 14, 16$ and 18 give a reasonably faithful indication of the power-law behaviour.

In figures 13(a, b) the normalized structure functions $\langle(\Delta u)^n\rangle/\langle u^2\rangle^{\frac{1}{2}n}$ are plotted logarithmically as functions of r/η with $n = 7, 8, 9, 10$ and 12 for the jet, $R_\lambda = 536$ (figure 13a) and $n = 7, 8, 9, 10, 12$ and 14 for the duct (figure 13b). As it is more

common to normalize by $\langle u^2 \rangle^{\frac{1}{2}}$ rather than V_K , the Reynolds number $R_L = \langle u^2 \rangle^{\frac{1}{2}} L/\nu$ is introduced in (12) in the form

$$\frac{\langle (\Delta u)^n \rangle}{\langle u^2 \rangle^{\frac{1}{2}n}} = C_n R_L^{-\frac{1}{2}n} \left(\frac{r}{\eta} \right)^{\zeta_n}. \quad (13)$$

The slopes calculated from LN and the β -model are drawn for orders 8 and 12 (with $\mu = 0.2$) for comparison. This indicates that structure-function measurements up to order 8 cannot decide between LN and the β -model, unless perhaps the extent of the inertial range is one to two decades. Orders larger than 12, on the other hand, clearly invalidate the β -model. Figure 13 re-emphasizes the importance of an objective criterion for determining the inertial range (see §4.1). A relatively small shift in the inertial zone can significantly affect the slopes and the conclusions!

Figure 13(c) contains even-order structure functions for $n = 8-18$ obtained in the jet at $R_\lambda = 852$. Orders 10 and 12 behave in a way similar to what is observed on figures 13(a, b). However, oscillations, which are only weakly manifested for $n = 10$ and 12, are rapidly amplified at larger n . Values of the exponents ζ_n given in table 2 were obtained from least-squares fits to all the data points in the inertial range. A comparison with LN and the β -model of the variation of the exponents ζ_n is given in figure 14. Results obtained previously by others, limited to $n \leq 9$ except for Vasilenko, Lyubimtsev & Ozmidov (1975), are also included. The experimental results for $n > 9$ do not support the linear behaviour suggested by the β -model. Up to order 12, LN is a remarkably good approximation to the data, and only structure functions for $n \geq 14$ underline the limitations of LN. The latter observation must be treated with some caution in view of our inability to ascertain with confidence the accuracy of the highest-order structure functions. With this qualification, LN, which is the only model with a quadratic dependence of the exponent that satisfies $\zeta_3 = 1$ and $\zeta_6 = 2 - \mu$, is a good approximation for the behaviour of the exponent for $n \lesssim 12$. The higher-order moments indicate that the distribution is at best only 'nearly lognormal'. In particular, Mandelbrot (1972) emphasizes the possible 'near identity' of low-order moments of different random variables which have strikingly different high-order moments. We should perhaps also recall that the general inequality derived by Novikov (1971; see also Monin & Yaglom 1975, p. 622),

$$\mu_{\frac{1}{3}n} \leq \frac{1}{3}n + \mu - 2 \quad (\frac{1}{3}n > 2),$$

excludes the quadratic dependence (3) implied by LN.

5.2. A μ -independent representation

Vasilenko *et al.* (1975) suggested a test of the theoretical models which does not depend on the numerical value of μ . This representation is of interest because there have been suggestions that μ might be variable with n (Frenkiel, Klebanoff & Huang 1979). The procedure is to define, using the inertial-range power-law distributions

$$\begin{aligned} \langle (\Delta u)^n \rangle &\sim r^{\frac{1}{3}n - \mu_{\frac{1}{3}n}}, \\ [\langle (\Delta u)^{2n} \rangle]^{\frac{1}{2}} &\sim r^{\frac{1}{3}n - \frac{1}{2}\mu_{\frac{2}{3}n}}, \end{aligned}$$

the function

$$F_{mn} = \frac{\langle (\Delta u)^{mn} \rangle}{[\langle (\Delta u)^{2n} \rangle]^{\frac{1}{2}m}} \sim r^{-\mu_{\frac{1}{3}mn} + \frac{1}{2}m\mu_{\frac{2}{3}n}}. \quad (14)$$

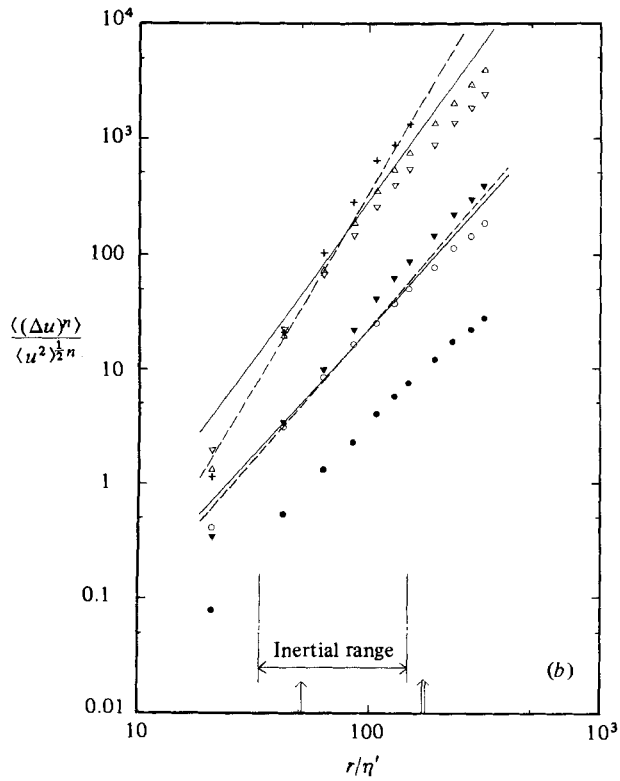
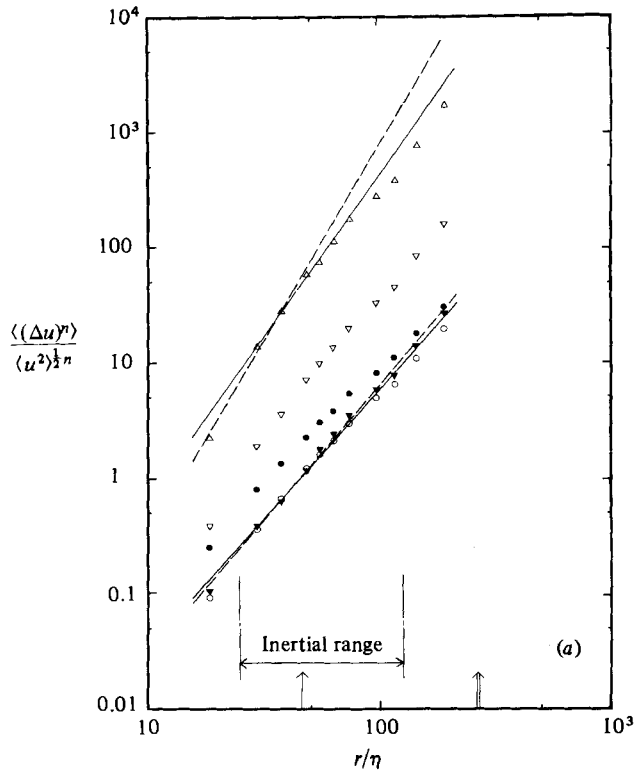


FIGURE 13(a, b). For caption see facing page.

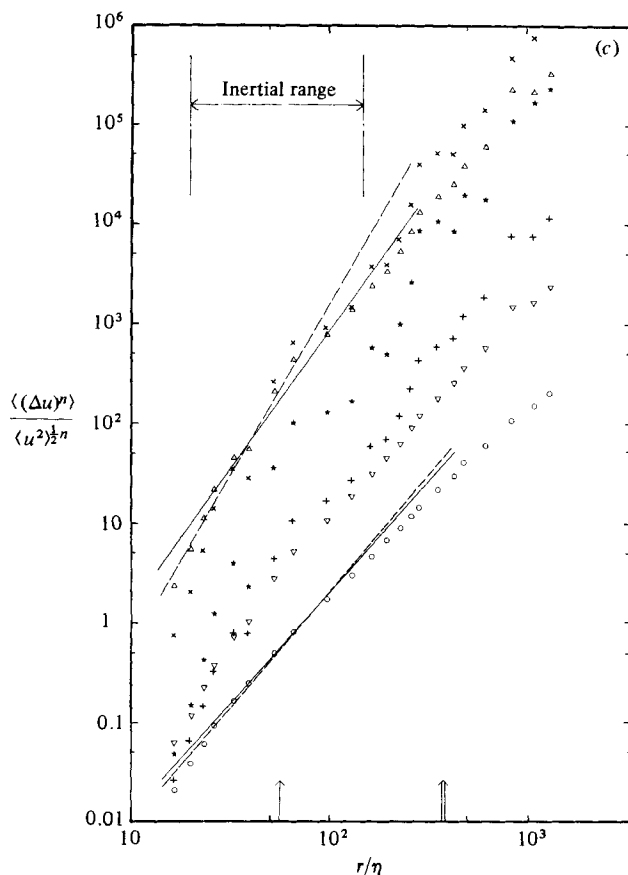


FIGURE 13. Inertial-range behaviour of structure functions $\langle(\Delta u)^n\rangle/\langle u^2\rangle^{\frac{n}{2}}$ with r/η for $n = 7-18$: \bullet , $n = 7$; \circ , 8; \blacktriangledown , 9; \triangledown , 10; \triangle , 12; $+$, 14; \times , 16; \star , 18. (a) Jet at $R_\lambda = 536$. (b) Duct flow at $R_\lambda = 515$. The twelfth and fourteenth order are divided by 10. (c) Jet at $R_\lambda = 852$. The fourteenth order is divided by 50, the sixteenth by 10 and eighteenth by 10^3 . The vertical chain-dotted lines indicate inertial-range limits. The slopes for orders 8 and 12 calculated from LN (—) and the β -model (---), $\mu = 0.2$, are indicated for reference.

We look for a relation of the type

$$F_{mn} \sim (F_{ln})^{\gamma_{m,l}}, \quad (15)$$

independent of r , which imposes on the constant $\gamma_{m,l}$ the constraint

$$\mu_{\frac{1}{2}mn} - \mu_{\frac{1}{2}ln} \gamma_{m,l} + \frac{1}{2}(l\gamma_{m,l} - m) \mu_{\frac{2}{3}n} = 0. \quad (16)$$

If a second-order polynomial

$$\mu_{\frac{1}{3}n} = \frac{1}{9}an^2 + \frac{1}{3}bn + c \quad (17)$$

is now introduced into (16), we obtain

$$2an^2[m(m-2) - l(l-2)\gamma_{m,l}] - 9c[(m-2) - (l-2)\gamma_{m,l}] = 0. \quad (18)$$

For a model that is linear in n , (18) yields

$$\gamma_{m,l} = \frac{m-2}{l-2}, \quad (19)$$

n	2	3	4	5	6	7	8	9	10	12	14	16	18
$R_\lambda = 515$ (duct)	0.71	1	1.33	—	1.8	—	2.27	—	2.64	2.94	3.32	—	—
$R_\lambda = 536$ (jet)	0.71	1	1.33	1.54	1.8	2.06	2.28	2.41	2.60	2.74	—	—	—
$R_\lambda = 852$ (jet)	0.71	1	1.33	1.65	1.8	2.12	2.22	2.52	2.59	2.84	3.28	3.49	3.71

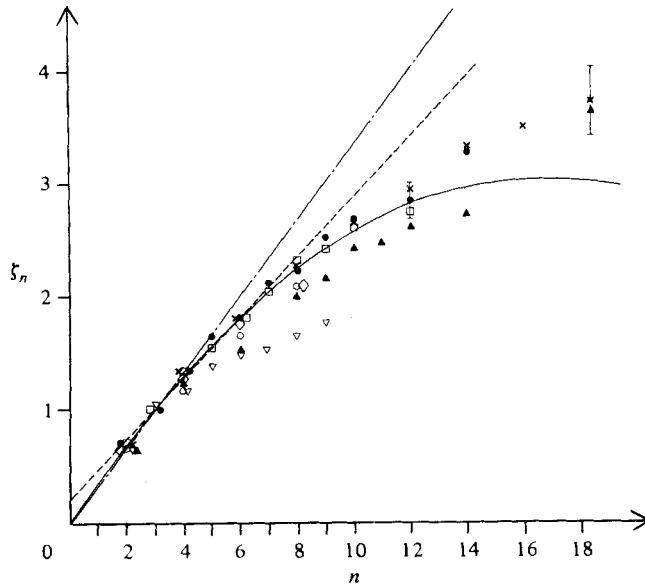
TABLE 2. Values of the exponent ζ_n for $2 \leq n \leq 18$ 

FIGURE 14. Variation of exponent ζ_n as a function of the order n . \bullet , $R_\lambda = 515$ (duct); \square , 536; \times , 852. Symbols \circ , \blacktriangle , ∇ , \diamond are respectively the exponents given by Mestayer (1980); Vasilenko *et al.* (1975); Van Atta & Park (1972); and Antonia *et al.* (1982*a*). The solid curve is LN with $\mu = 0.2$, the dotted curve the β -model and the chain-dotted line Kolmogorov's (1941) model.

and for a quadratic model with $c = 0$ in (18)

$$\gamma_{m,l} = \frac{m(m-2)}{l(l-2)}. \quad (20)$$

Substituting (19) into (15) for $m = 1$ and $l = 3$ and 4, we obtain, for a linear model,

$$F_n \sim (F_{4n})^{-\frac{1}{2}}, \quad F_n \sim (F_{3n})^{-1}. \quad (21)$$

For the same values of m and l , the quadratic model yields after substituting (20) into (15)

$$F_n \sim (F_{4n})^{-\frac{1}{6}}, \quad F_n \sim (F_{3n})^{-\frac{1}{3}}. \quad (22)$$

Figures 15(a, b) are log-log plots of F_n versus F_{4n} (figure 15a) and F_n versus F_{3n} (figure 15b), for $n = 2, 3$ and 4, the present three experimental conditions and all values of r in the inertial range. The experimental data in figures 15(a, b) are in reasonable agreement with LN up to order 12 ($n = 3$ and 4 in the presentations). However, the

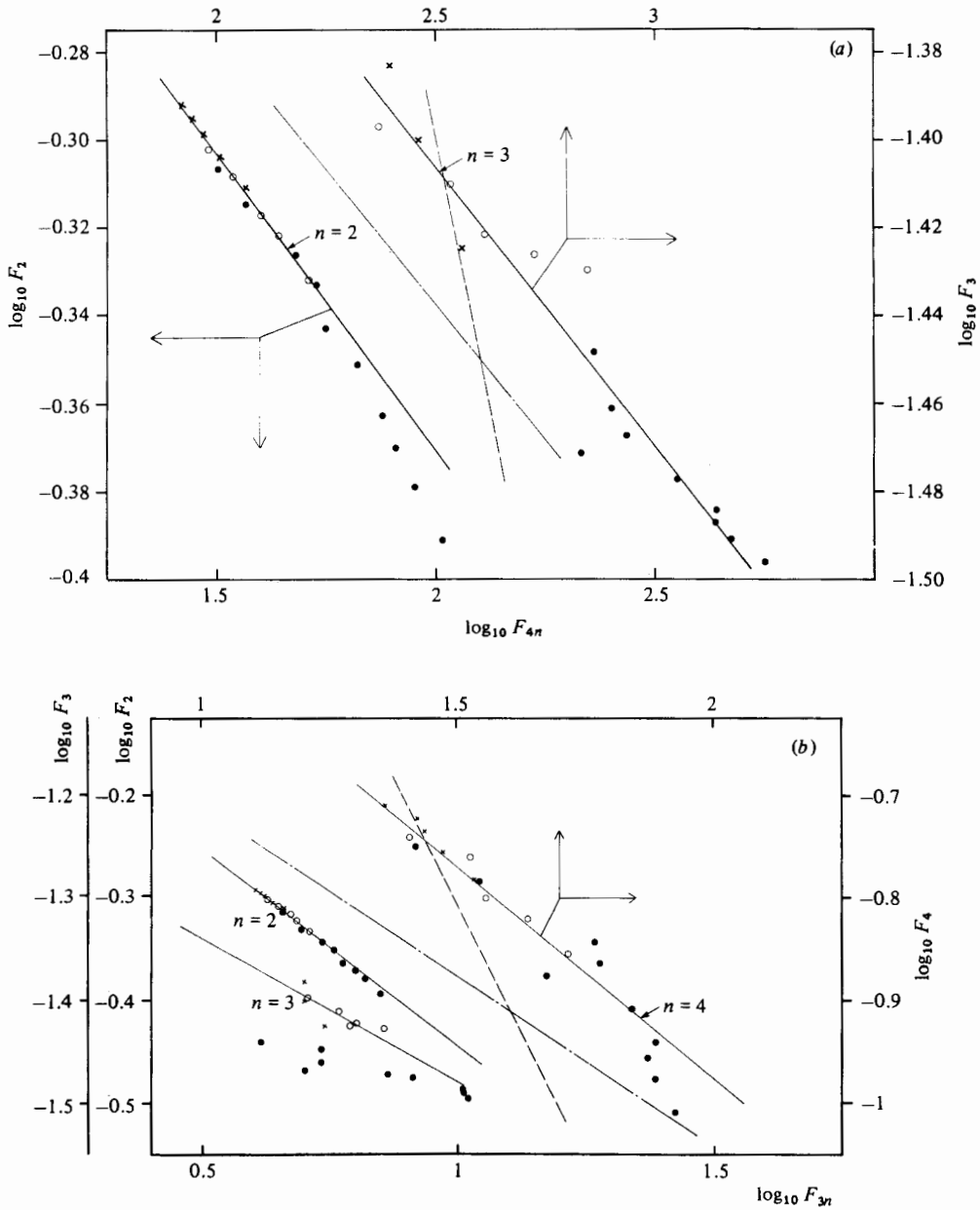


FIGURE 15. Plots of moments F_n as a function of (a) F_{4n} ($n = 2, 3$); (b) F_{3n} ($n = 2, 3, 4$) for the data taken from all three flow conditions: \times , duct, $R_\lambda = 515$; \circ , jet, $R_\lambda = 536$; \bullet , jet, $R_\lambda = 852$. — — —, LN β -model; — least-square fit to experimental data.

slopes depend weakly on the order n , in contrast with a true quadratic model, which requires that $\gamma_{m,l}$ does not depend on n . This observation confirms the inferences made from figure 14 that the distribution is not lognormal in the strict sense. Because of the deviation from a true quadratic behaviour the possibility of matched two-segment linearity in n as suggested by Schertzer & Lovejoy (1983) cannot be ruled out entirely.

6. Conclusions

To distinguish between dissipation models, such as the lognormal model and the dynamical β -model developed by Frisch *et al.* (1978) relatively high-order moments of the velocity derivative or the velocity structure function are required as well as an accurate determination of the intermittency parameter μ . In this paper we have focused mainly on the velocity structure function and measured moments of order as high as 14 in a duct flow and 18 for a moderately high-Reynolds-number axisymmetric jet. These relatively high-order moments necessitated a careful appraisal of the experimental uncertainty, in particular the error involved in determining the extreme tails of the probability density function. Convergence-time considerations and the requirement of convergence for the moment integrands indicated that satisfactory accuracy could not be maintained for moments of order higher than about 12. However, it was also noted that the inertial range slope associated with higher-order moments should not be significantly affected by the decreasing accuracy of these moments. As a result, the behaviour of moments as high as 18 is believed to be given to fair accuracy.

An important consideration in estimating the inertial range power-law exponents accurately is the careful definition of the bounds of the inertial range. It is argued that the second-order moment is influenced by the intermittency of the dissipation field and may not be an unambiguous indicator of the inertial range. The approach adopted is to consider both second- and third-order moments, the latter remaining unaffected by intermittency.

The sixth-order structure functions indicate a value of μ of 0.2 (± 0.05). This estimate is, to within the conjecture of Frisch *et al.* (1978), model-independent and not as ambiguous as that derived from fluctuations of the velocity derivative squared. Autocorrelations of these non-centred fluctuations lead to the same value of μ . Once μ is firmly established, a meaningful comparison between lognormal and β -models can be carried out. Figures 14 and 15 underline that the linear variation of the β -model is not supported by the data. Although moments up to order 12 are closely approximated by the lognormal model, the deviation from it for higher-order moments seems genuine, notwithstanding the experimental uncertainty of estimating these moments.

R. A. A. acknowledges the kind hospitality at the IMG and the support of the Australian Research Grants Scheme.

The work was financially supported by the DRET under contracts 81/639 and 83/314. We are particularly grateful to J.-P. Barbier-Neyret for his help with the measurements and the data acquisitions. Comments by A. M. Yaglom on a preliminary version of the paper were most valuable.

REFERENCES

- ANTONIA, R. A., SATYAPRAKASH, B. R. & HUSSAIN, A. K. M. F. 1980 *Phys. Fluids* **23**, 695–700.
 ANTONIA, R. A., SATYAPRAKASH, B. R. & CHAMBERS, A. J. 1982a *Phys. Fluids* **25**, 29–37.
 ANTONIA, R. A., SATYAPRAKASH, B. R. & HUSSAIN, A. K. M. F. 1982b *J. Fluid Mech.* **119**, 55–89.
 ANTONIA, R. A. & VAN ATTA, C. W. 1978 *Phys. Fluids* **21**, 1096–1099.
 CHORIN, A. J. 1982 *Commun. Math. Phys.* **83**, 517–535.
 COMTE-BELLOT, G. 1965 *PST Ministère de l'Air* **419**, Paris.
 CORRSIN, S. 1962 *Phys. Fluids* **5**, 1301–1302.

- FRENKIEL, F. N. & KLEBANOFF, P. S. 1975 *Boundary-Layer Meteor.* **8**, 173–200.
- FRENKIEL, F. N., KLEBANOFF, P. S. & HUANG, T. 1979 *Phys. Fluids* **22**, 1606.
- FRISCH, U., SULEM, P.-L. & NELKIN, M. 1978 *J. Fluid Mech.* **87**, 719–736.
- FUJISAKA, H. & MORI, H. 1979 *Prog. Theor. Phys.* **62**, 54.
- GAGNE, Y. 1980 Thèse Docteur-Ingénieur, Université Scientifique et Médicale et Institut National Polytechnique de Grenoble.
- GAGNE, Y. & HOPFINGER, E. J. 1979 In *Proc. 2nd Symp. on Turbulent Shear Flow, London*.
- HENTSCHEL, H. G. E. & PROCACCIA, I. 1982 *Phys. Rev. Lett.* **49**, 1158.
- KOLMOGOROV, A. N. 1941 *C.R. Acad. Sci. USSR* **30**, 301–305.
- KOLMOGOROV, A. N. 1962 *J. Fluid Mech.* **13**, 82–85.
- KRAICHNAN, R. H. 1974 *J. Fluid Mech.* **72**, 305–330.
- LUMLEY, J. L. 1970 *Stochastic Tools in Turbulence*. Academic.
- MANDELBROT, B. 1972 In *Statistical Models and Turbulence* (ed. M. Rosenblatt & C. Van Atta). Lecture Notes in Physics, vol. 12, pp. 333–351. Springer.
- MANDELBROT, B. 1976 In *Turbulence and Navier Stokes Equations* (ed. R. Temam). Lecture Notes in Mathematics, vol. 565, pp. 121–145. Springer.
- MARÉCHAL, J. 1970 Thèse Docteur-Ingénieur, Université Scientifique et Médical de Grenoble.
- MATHIEU, J. & COMTE-BELLOT, G. 1958 *C.R. Acad. Sci. Paris* **246**, 2220–2223.
- MESTAYER, P. 1980 Thèse Docteur ès Sciences Physiques, Université d'Aix-Marseille II.
- MONIN, A. S. & YAGLOM, A. M. 1975 *Statistical Fluid Mechanics: Mechanics of Turbulence*, vol. 2. MIT Press.
- NELKIN, M. 1981 *Phys. Fluids* **24**, 556–557.
- NELKIN, M. & BELL, T. L. 1978 *Phys. Rev.* **A17**, 363–369.
- NOVIKOV, E. A. 1971 *Prikl. Math. Mekh.* **35**, 266–277.
- NOVIKOV, E. A. & STEWART, R. W. 1964 *Izv. Geophys.* **3**, 408–413.
- OBUKHOV, A. M. 1962 *J. Fluid Mech.* **13**, 77–81.
- SAFFMAN, P. G. 1968 *Lectures on Homogeneous Turbulence: Topics in Nonlinear Physics*. Springer.
- SCHERTZER, D. & LOVEJOY, S. 1983 *Reprints of IUTAM Symp. on Turbulence and Chaotic Phenomena in Fluids, Kyoto*, p. 141.
- SREENIVASAN, K. R., CHAMBERS, A. J. & ANTONIA, R. A. 1978 *Boundary-Layer Meteor.* **14**, 341–359.
- TENNEKES, H. 1968 *Phys. Fluids* **11**, 669–671.
- TENNEKES, H. & LUMLEY, J. L. 1972 *A First Course in Turbulence*. MIT Press.
- TENNEKES, H. & WYNGAARD, J. C. 1972 *J. Fluid Mech.* **55**, 93–103.
- VAN ATTA, C. W. & CHEN, W. Y. 1970 *J. Fluid Mech.* **44**, 145–159.
- VAN ATTA, C. W. & PARK, J. 1972 In *Statistical Models and Turbulence* (ed. M. Rosenblatt & C. Van Atta). Lecture Notes in Physics, vol. 12, pp. 402–426. Springer.
- VASILENKO, V. M., LYUBIMTSEV, M. N. & OZMIDOV, R. V. 1975 *Izv. Atmos. Ocean. Phys.* **11**, 926–932.
- WYGNANSKI, I. & FIEDLER, H. 1969 *J. Fluid Mech.* **38**, 577.
- WYNGAARD, J. C. & PAO, Y. H. 1972 In *Statistical Models and Turbulence* (ed. M. Rosenblatt & C. Van Atta). Lecture Notes in Physics, vol. 12, pp. 384–401. Springer.
- YAGLOM, A. M. 1966 *Sov. Phys. Dokl.* **11**, 26–29.